



Titre: Physics-informed Neural Network to predict kinetics of biodiesel production in microwave reactors

Auteurs: Valérie Bibeau, Daria Camilla Boffito, & Bruno Blais

Date: 2024

Type: Article de revue / Article

Référence: Bibeau, V., Boffito, D. C., & Blais, B. (2024). Physics-informed Neural Network to predict kinetics of biodiesel production in microwave reactors. Chemical Engineering and Processing-Process Intensification, 196, 109652 (9 pages).
Citation: <https://doi.org/10.1016/j.cep.2023.109652>

 **Document en libre accès dans PolyPublie**

Open Access document in PolyPublie

URL de PolyPublie: <https://publications.polymtl.ca/57565/>
PolyPublie URL:

Version: Version finale avant publication / Accepted version
Révisé par les pairs / Refereed

Conditions d'utilisation: Creative Commons Attribution-Utilisation non commerciale-Pas d'oeuvre dérivée 4.0 International / Creative Commons Attribution-NonCommercial-NoDerivatives 4.0 International (CC BY-NC-ND)
Terms of Use:

 **Document publié chez l'éditeur officiel**

Document issued by the official publisher

Titre de la revue: Chemical Engineering and Processing-Process Intensification (vol. 196)
Journal Title:

Maison d'édition: Elsevier science sa
Publisher:

URL officiel: <https://doi.org/10.1016/j.cep.2023.109652>
Official URL:

Mention légale:
Legal notice:

Physics-informed Neural Network to Predict Kinetics of Biodiesel Production in Microwave Reactors

Valérie Bibeau^{a,b}, Daria Camilla Boffito^{b,c}, Bruno Blais^{*a}

^a*Department of Chemical Engineering, Research Unit for Industrial Flows Processes (URPEI), Polytechnique Montréal, C.P. 6079, Succ. "CV", Montréal, H3C 3A7, Québec, Canada*

^b*Department of Chemical Engineering, Engineering Process Intensification and Catalysis (EPIC), Polytechnique Montréal, C.P. 6079, Succ. "CV", Montréal, H3C 3A7, Québec, Canada*

^c*Canada Research Chair in Engineering Process Intensification and Catalysis (EPIC), Polytechnique Montréal, C.P. 6079, Succ. "CV", Montréal, H3C 3A7, Québec, Canada*

Abstract

Microwaves are a process intensification (PI) method to deliver energy to reactive systems. Microwaves act directly on molecules' dipolar moment, generating volumetric heating that allows temperature to rise rapidly, which directly impacts the overall rate of a reaction. Because reaction rates adhere to non-linear rate laws, predicting them is challenging. We use a Physics-informed Neural Network (PINN), a physics-driven model, to identify the reaction kinetics of a biodiesel production process. PINNs perform a regression on very few experimental data points and try to fit the physics at hand. We use a microwave reactor with a constant power input to perform the transesterification reaction, measure the infrared temperature and analyze the concentration of glycerides using GC-FID at different reaction times. We train the PINN to predict the reaction rates with respect to the Arrhenius equation. Results show that the PINN successfully identifies the rate constants, including their temperature dependency. Furthermore, the PINN can extrapolate its predictions to other power inputs without ever seeing the concentration data, generating a digital twin of the microwave-assisted reaction.

Keywords: Microwave, Reaction kinetics, PINN, Digital twin

1. Introduction

Engineers mostly design chemical plants based on the "big is best" paradigm to achieve economies of scale [1]. This process design is sequential and operation-orientated, leading to plants with high volume footprint [1, 2]. Process intensification (PI) is a paradigm shift that either designs new or retrofits existing processes into more compact and more efficient ones [3]. One of PI's approaches is enhancing heat transfer with alternative energy vectors [2]. Microwaves are a form of electromagnetic radiation that generates volumetric heating [4]. They

interact directly with the material at the molecular level, more specifically molecules that have a polar moment. Under microwave emission, dipole forces within molecules try to align the electromagnetic field, making them rotate. This spin results in the dissipation of heat through the internal resistance of rotation [4]. Unlike conductive heating, volumetric heating is more efficient and allows for faster reactions [5, 6]. Kinetics modeling measures the contribution of microwaves on reaction rates, which is key to design, optimize and control microwave reactors [7].

Microwave technology shows great potential in the field of biodiesel production. The main way to produce biodiesel is by transesterification because of its high yields, lower cost, and short reaction time [8]. Transesterification consists of transforming oils (glycerides) into methyl esters (biodiesel) and glycerol using ethanol or methanol [9]. Because alcohols are polar molecules, microwave irradiation increases their level of polarization and accelerates the transesterification reaction [10]. Moreover, a study of synergistic ultrasound and microwave for in-situ biodiesel production demonstrates enhanced reaction rates through the gamma irradiation of the feedstock during the pre-treatment process [11]. It shows that the reaction can be done under 30 min, which is 3 times faster than conventional heating [9, 11].

Reaction kinetics frequently use rate laws that relate a reaction rate to species concentration (e.g. [A] and [B]), stoichiometry and rate constants k :

$$\text{Rate} = k[A]^x[B]^y \quad (1)$$

Assuming that reactions are homogeneous, and using a mass balance on the species, we can predict the evolution of concentration over time with a set of ordinary differential equations (ODEs).

Because most reactions are reversible (limited by thermodynamic equilibrium), and include intermediates, closed-form analytical solutions for the set of ODEs can seldom be obtained [12]. Modeling strategies exist to reduce the complexity of reactions and thus the number of rate constants to obtain, such as lumping, quasi-steady state and quasi-equilibrium approximations [13]. Moreover, some kinetic modeling strategies couple mass and energy balances to reduce the number of parameters to be estimated by non-linear regression [14]. Other strategies, like Response Surface Methodology (RSM), enable a reduction in the number of experimental runs required, leading to minimal efforts, time and resources [15]. On the other hand, a more detailed kinetics approach, such as composition modeling techniques, tries to preserve the specifics of chemicals at the molecular scale [13]. This strategy, although accurate, is difficult to leverage when there are multiple reaction intermediates [16]. Thus, the challenge is to find a compromise between the use of experimental data and the complexity level of the reaction mechanisms considered.

Digital twins can be generated by merging a physics-based model with neural networks [17]. In chemical engineering, digital twins are made for design, optimization, process control, predictive maintenance and more [18]. They try

to replicate, numerically, the functional services of a physical entity, like a small-scale microwave reactor [19, 20].

In this work, we leverage Physics-informed Neural Networks (PINNs) to identify the reaction kinetics of a multi-step reaction that occurs in a microwave reactor. The reaction we study is the production of biodiesel through transesterification of canola oil. First, we present an overview of PINNs. Then, we present the methodology for extracting the concentration data and the temperature data of the transesterification reaction done under non-isothermal conditions. We also present the physical model, which is the ODEs that the PINN solves and the rate constants that it evaluates. We explain in detail the architecture of the PINN that identifies the reaction rates and generalizes to other microwave power values. Finally, we illustrate and discuss the predictions of the PINN and evaluate its capacity to extrapolate to other operating conditions, making it a promising choice for applications related to digital twins.

1.1. Physics-informed Neural Networks

PINNs encode in their training the governing equations that describe the evolution of a physical quantity over time and/or space. Consequently, PINNs approximate partial differential equations (PDEs) or ODEs [21]. To estimate the solution of an ODE specifically, we train a PINN by minimizing a loss function \mathcal{L} . The loss combines the mean squared error of the residual form of the ODE (MSE_f) evaluated at different collocation points in time and the mean squared error of the initial condition and measurements (MSE_u) [22]:

$$\mathcal{L} = \text{MSE}_u + \text{MSE}_f \quad (2)$$

where,

$$\text{MSE}_u = \sum_i^{N_u} |u_i - \hat{u}_i|^2 \quad (3)$$

$$\text{MSE}_f = \sum_j^{N_f} |f(t_j)|^2 \quad (4)$$

with N_u the number of labeled data points, u_i the predicted solution of the ODE, \hat{u}_i the initial condition and the measurements, N_f the number of collocation points, t_j a specific collocation point in time and $f(t_j)$ the evaluation of the residual form of the ODE at the collocation point. The residual form f is:

$$f := u_t + f(u, \lambda) \quad (5)$$

with u_t the derivative of the solution over time, λ the parameters (or constants) of the ODE and $f(u, \lambda)$ the right-hand side of the ODE, which could be non-linear with respect to u and λ .

We present a typical PINN's architecture for solving an ODE in Figure 1. The PINN predicts u at each temporal collocation point using the neural network. To calculate u_t , we perform automatic differentiation (AD) that calculates the overall derivative by combining known derivatives through the chain rule [23]. Finally, the PINN updates the weights of its network iteratively using the gradient descent algorithm until a targetted loss is reached [24].

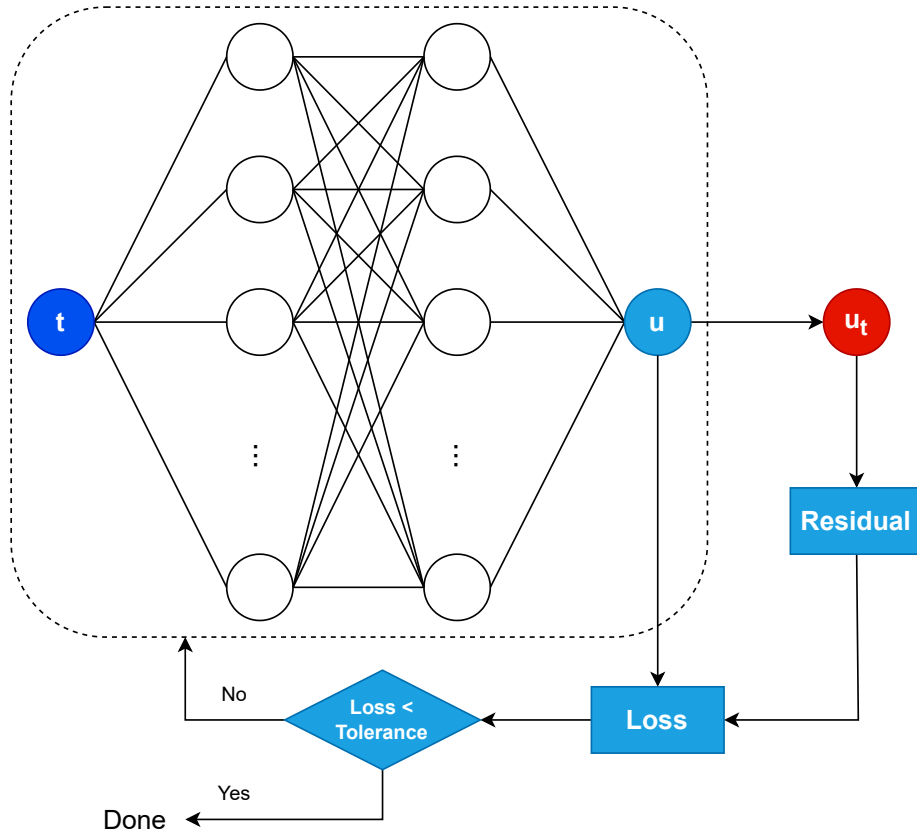


Figure 1: PINN's architecture.

PINNs can solve inverse problems where parameters of PDEs or ODEs are unknown. Using gradient descent, PINNs are able to discover the parameters λ from Equation 5 during training [22]. For example, a PINN solves a catalytic CO_2 methanation reaction and discovers an unknown effectiveness factor involved in the reaction kinetics [25]. In the context of reaction kinetics, a PINN could be used to solve the inverse mass balance problem and identify all the rate constants and their dependence on temperature. If we want to create a

digital twin, this PINN should generalize to multiple operating conditions of the microwave reactor. To the best of our knowledge, this approach has not yet been used and the present work addresses this issue.

2. Methodology

We present the methodology behind the extraction of the data for the discovery of the ODEs describing the reaction rates of the transesterification reaction. First, we get the concentration data at different reaction times from gas chromatography (GC). Second, an infrared (IR) sensor or a ruby ball probe measures the temperature. Finally, we describe the physical model of the reaction, or the ODEs describing the reaction kinetics and the global energy balance.

2.1. Concentration and temperature data

We perform the transesterification reaction in an Anton Paar Monowave 400 reactor, which operates as a single mode system. Figure 2 illustrates the functional parts of the microwave reactor [26]. The reaction uses canola oil (of the brand President’s Choice, available in grocery stores in Québec, Canada) and methanol (MeOH) with a molar ratio of 1:6. We choose canola oil for its high content in oleic acid, which produces biodiesel with better cold flow properties, and its low melting point, making the oil fluid at room temperature [27]. The catalyst is sodium hydroxyde (NaOH) and its concentration is 0.8% w/w [28].

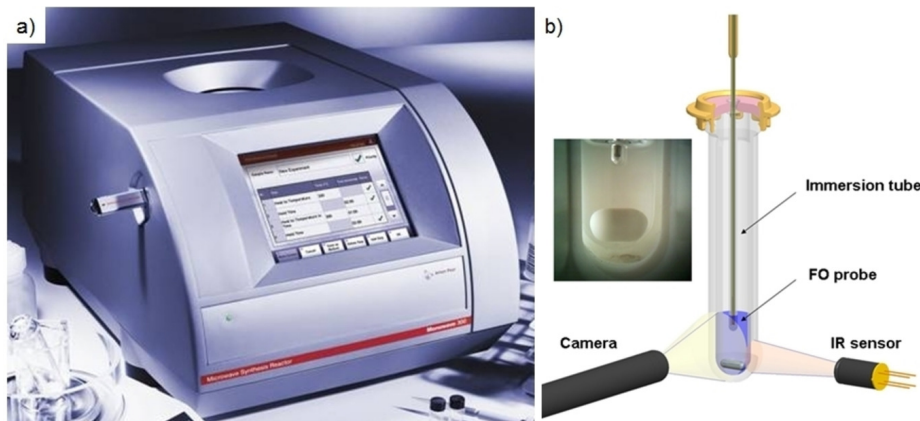


Figure 2: Anton Paar reactor. a) Microwave reactor from the outside. b) Inside of the reactor.

We agitate the reagents to prevent phase separation and set a constant magnetic agitation of 600 rpm during the reaction [29, 30]. We set a constant power input (amount of energy put into the reactor) of 4, 5 and 6 Watts until the mixture’s temperature reaches 65 °C, the temperature at which the methanol starts to evaporate and the reaction kinetics are optimal [31]. The time it takes to reach 65 °C is approximately 10 min for a power of 4 W, 6 min for 5 W and 4 min for 6 W. We also measure the concentration of the species at

multiple times before the temperature of 65 °C is reached. To avoid any loss of reaction mass, we cool the products by quenching them in a cold bath. Table 1 summarizes the experiments done in the microwave reactor with reagents volume and catalyst mass.

Exp. no.	Power input (W)	Reaction time (s)	Canola oil volume (± 0.05 mL)	Methanol volume (± 0.05 mL)	Catalyst mass (± 0.0001 g)
1	4	60	5	1.3	0.0450
2	4	120	5	1.3	0.0450
3	4	240	5	1.3	0.0450
4	4	360	5	1.3	0.0450
5	4	600	5	1.3	0.0450
6	5	60	5	1.3	0.0450
7	5	120	5	1.3	0.0450
8	5	240	5	1.3	0.0450
9	5	360	5	1.3	0.0450
10	6	60	5	1.3	0.0450
11	6	120	5	1.3	0.0450
12	6	240	5	1.3	0.0450

Table 1: Power input of the microwave, reaction time of the experiments, mass and volume of reagents.

We extract a sample of the reaction products in order to analyze their components using gas chromatography with flame ionization detection (Scion GC-FID). Following the EN-14105 procedure, we mix the sample with 100 μ L of MSTFA for derivatization and 100 μ L of tricaprln as the internal standard for glycerides analysis [32, 33, 34].

With the chromatogram computed by the GC-FID, we evaluate the corrective factor (C_F) of the glycerides, which is the reciprocate of the relative response factor of the detector:

$$C_F = \frac{A_x m_{IS}}{A_{IS} m_x} = \frac{A_x C_{IS} V_{IS}}{A_{IS} m_x} \quad (6)$$

with A_x the peak area of the glycerides, A_{IS} the peak area of the internal standard, C_{IS} the concentration of the internal standard (8 mg mL⁻¹), V_{IS} the volume of the internal standard and m_x the mass of the sample [34].

Knowing the total mass m , the molar mass M of the glycerides and the volume of the solution V , it is easy to retrace the molar concentration (in mol L⁻¹) over each reaction time from the corrective factor [34]. The final concentration is:

$$C = C_F \times \frac{mM}{V} \quad (7)$$

We produce 3 replicates of the experiments presented in Table 1 to evaluate the error of the concentration data and the reproducibility of the methodology. This results in a total of 36 reaction samples being generated. The error obtained on the concentration data varies between 2 and 50%. Using the same GC-FID, we calculate the initial concentration (IC) of each glyceride from raw canola oil. Table 2 presents the molecular weight (MW) of each compound [35] and their respective concentration before starting the reaction.

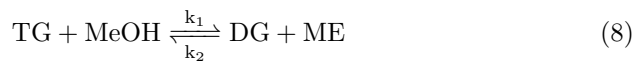
Glyceride	MW (g mol ⁻¹)	IC (mol L ⁻¹)
TG	885	0.61911
DG	621	0.04000
MG	357	0.00039

Table 2: Molecular weights and initial concentrations of glycerides.

As for the temperature, the reactor has an infrared (IR) sensor that detects the temperature of the sample inside the vial. The numerical output of the Anton Paar reactor is the temperature in degree Celsius (°C) at each second of operation.

2.2. Physical model

The transesterification reaction occurs in three consecutive steps where the triglycerides (TG) break down into diglycerides (DG), then into monoglycerides (MG) and finally into glycerol (G). With an excess of methanol (MeOH) and sodium hydroxide (NaOH) as the catalyst, each step produces methyl esters (ME) or biodiesel. All reactions are reversible:



with k_1 , k_3 and k_5 the rate constants of the forward reactions and k_2 , k_4 and k_6 the rate constants of the reverse reactions [36].

Using rate laws and species balance, we obtain the following set of ODEs:

$$\frac{d[TG]}{dt} = -k_1[TG] + k_2[DG][ME] \quad (11)$$

$$\frac{d[DG]}{dt} = -k_2[DG][ME] + k_1[TG] - k_3[DG] + k_4[MG][ME] \quad (12)$$

$$\frac{d[MG]}{dt} = -k_4[MG][ME] + k_3[DG] - k_5[MG] + k_6[G][ME] \quad (13)$$

$$\frac{d[ME]}{dt} = +k_1[TG] - k_2[DG][ME] + k_3[DG] - k_4[MG][ME] + k_5[MG] - k_6[G][ME] \quad (14)$$

$$\frac{d[G]}{dt} = -k_6[G][ME] + k_5[MG] \quad (15)$$

$$(16)$$

We suppose that all forward reactions are pseudo-first order reactions and we reduce the second-order reactions into first-order. This hypothesis is valid because the methanol is in high excess [36].

Rate constants k are dependant on temperature. They follow the Arrhenius equation:

$$k = A \exp\left(\frac{-E_a}{RT}\right) \quad (17)$$

with A the pre-exponential factor, E_a the activation energy, R the gas constant and T the temperature.

Because the scale of the pre-exponential factor A and the activation energy E_a is usually high, the training of the PINN is very stiff and it is difficult to achieve convergence. To simplify the model, we linearize the Arrhenius equation using a first-order Taylor expansion:

$$k(T) = k(\bar{T}) + \left. \frac{dk(T)}{dT} \right|_{T=\bar{T}} \frac{(T - \bar{T})}{1!} + \dots \quad (18)$$

$$k(T) = A \exp\left(\frac{-E_a}{R\bar{T}}\right) + A \exp\left(\frac{-E_a}{R\bar{T}}\right) \left(\frac{E_a}{R\bar{T}^2}\right) (T - \bar{T}) \quad (19)$$

$$k = k' + k''(T - \bar{T}) \quad (20)$$

with k' and k'' respectively the Arrhenius equation estimated at the mean temperature \bar{T} of the products during the reaction and the first derivative of the Arrhenius equation evaluated at \bar{T} .

Furthermore, for the evolution of the temperature over time, we suppose that it follows a simplified first-degree ODE:

$$\frac{dT}{dt} = \varepsilon P + c_1 T + c_2 \quad (21)$$

with P the power of the microwave reactor, ε the absorbance of the microwave energy by the reaction, the constants c_1 and c_2 that represents respectively the heat loss of the microwave reactor, following Newton’s law of cooling that is dependant on temperature, and the reaction source term. We assume the source term c_2 to be constant in order to reduce complex dependencies between temperature evolution and glycerides conversion.

The purpose of the PINN is to predict concentration and temperature over time using these previous ODEs as physical constraints. In addition, the PINN estimates the unknown rate constants of each reaction (k' and k'') as well as the constants from the energy balance (ε , c_1 and c_2) for a total of 15 trainable parameters. Having the data and the physics at hand, we present in the next section the final architecture of the PINN.

2.3. PINN implementation

We utilize grid search analysis for hyperparameter optimization, assessing the performance of the PINN across a specified hyperparameter space where both the number of layers and nodes are varied. The final PINN model that gave the lowest total MSE has an input layer of 2 neurons, 3 hidden layers of 64 neurons and an output layer of 6 neurons. We present the architecture of the PINN in Figure 3. The input layer includes the time t and the microwave power P . The number of instances, or the length of the features vector, is the number of collocation points discretized in the time domain. The power is a discrete value, either 4, 5 or 6 W. This feature differentiates the temperature evolution and therefore the concentration evolution based on an essential operating condition of the microwave.

As for the outputs, we associate 5 neurons to the species concentrations, which are [TG], [DG], [MG], [G] and [ME]. We associate the last neuron with the temperature. By doing so, the PINN predicts the concentrations and the temperature over time in synch.

The loss includes the mean squared errors of the residuals of the ODEs described in the physical model:

$$\text{MSE}_r = \frac{1}{N_r} \sum_i^{N_r} |r(t_i, P_i)|^2 \quad (22)$$

$$\text{MSE}_g = \frac{1}{N_g} \sum_i^{N_g} |g(t_i, P_i)|^2 \quad (23)$$

with r the residuals of the ODEs describing the concentration evolution of all species over time, g the residual of the ODE describing the temperature

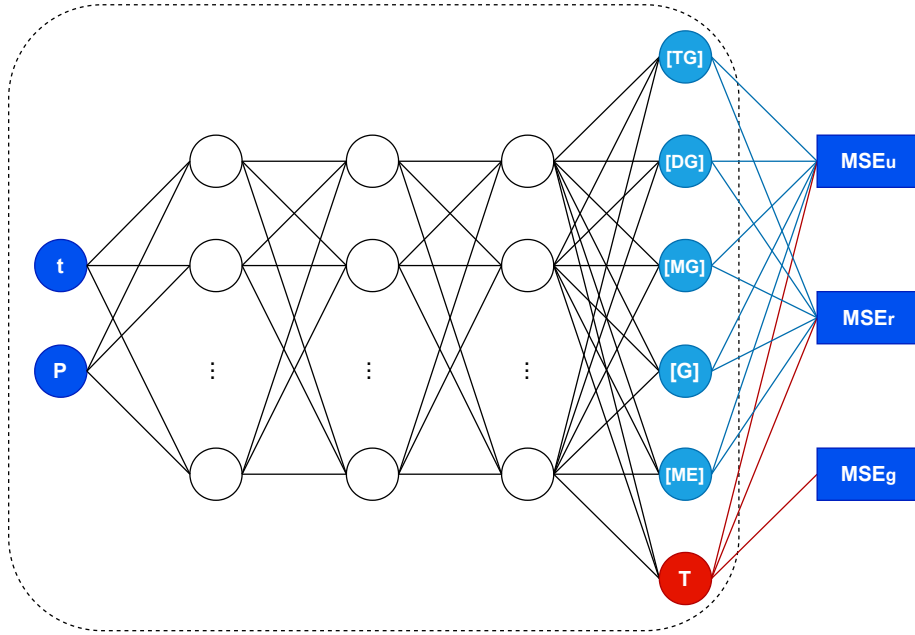


Figure 3: Reaction kinetics architecture.

evolution over time, N_r and N_g the number of collocation points where we evaluate the ODEs.

Table 3 shows the time domain and the number of collocation points (N_r and N_g) for each microwave power. We refine the discretization of the time domain to have a collocation point every half-second in order to better detect the fast transition region of the transesterification reaction [37, 38].

Power input (W)	Time domain (s)	Number of collocation points
4	[0,600]	1201
5	[0,360]	721
6	[0,240]	481

Table 3: Time domain and number of collocation points for each microwave power.

Solving an inverse problem where the physics is incomplete, we need to make the loss landscape more conducive to finding a solution. To do so, we evaluate the mean squared errors of the concentration data and the temperature data:

$$\text{MSE}_u = \frac{1}{N_C} \sum_i^{N_C} |C(t_i, P_i) - \hat{C}_i|^2 + \frac{1}{N_T} \sum_i^{N_T} |T(t_i, P_i) - \hat{T}_i|^2 \quad (24)$$

with C the concentration predicted by the PINN for a specific time and power (t_i, P_i), T the temperature predicted by the PINN for the same instance, \hat{C}_i and

\hat{T}_i the values coming from the experiments, N_C the number of concentration data, N_T the number of temperature data. N_C includes all replicates of the experiments in Table 1 and the initial condition of the canola oil. N_T depends on the sampling frequency of the IR temperature, which is 1 per second and includes the replicates of the full-time reaction experiments.

By combining the MSE_u , MSE_r and MSE_g , we obtain the final loss function \mathcal{L} of the PINN:

$$\mathcal{L} = \text{MSE}_u + \eta_r \text{MSE}_r + \eta_g \text{MSE}_g \quad (25)$$

with η_r the regularization parameter on the loss of the concentrations ODEs and η_g the regularization parameter on the loss of the temperature ODE.

Regularization plays a key role in PINN. It allows us to put more emphasis on penalizing the residuals compared to the MSE of the data. In other words, the PINN enforces the given physical constraints to satisfy the ODEs [39, 40]. First, we train the PINN with a low regularization parameter so that the PINN learns mostly from the data. This alleviates the complexity of the loss landscape (the shape of the loss in all feature dimensions) caused by the physics. Gradually, we increase the regularization parameter so that the PINN leads to solutions that satisfy the physics [41].

Finally, we train the PINN for 1M epochs on GPUs from Digital Research Alliance of Canada clusters. We use the tanh function to activate the hidden neurons of the PINN and we use the Adam optimizer [42] for the gradient algorithm. All experimental data, programming implementation of the PINN and training procedures are available in an open-access Github repository [43].

3. Results and Discussion

We present the predictions of the PINN and analyze them in two main fashion. First, we demonstrate the impact of the regularization parameter η_r on the PINN’s predictions. Second, we use all data available to identify as closely as possible the rate constants that dictate the reaction kinetics. Finally, we remove some concentration data and try to predict the concentration evolution over time, being closer to a physics-driven model. By doing so, we try to prove that it is possible to extrapolate the PINN’s predictions to other power inputs, making the PINN a digital twin of the microwave reactor.

3.1. Regularization

For regularization, we increase η_r from 5, 50, 500 and finally to 5000 progressively each 25,000 epochs. The moment we change η_r , the PINN continues its training by minimizing a different loss topology that is more physics-based. To understand and evaluate how the PINN behaves with regularization, we take the rate constants k (or λ) predicted by the PINN every 25,000 epochs and we inject them in a fourth-order Runge-Kutta numerical method for the ordinary

differential equations [44]. As for η_g , the parameter is set to 1 during the training. Equation 21 neglects multiple components of the physics (heat of reaction, changes in specific heat, etc.) and is overly simplified. A decrease in the regularization diminishes our confidence in the accuracy of the temperature ODE, thereby making the PINN more inclined to conform closely to the data.

Figure 4 shows the PINN predictions of the TG concentration over time when the regularization η_r is increased during the training. The predictions are compared to the numerical ODEs. We see that for a lower regularization parameter value ($\eta_r = 5$) the PINN fits more the data. Indeed, the rate constants predicted by the PINN solve ODEs that are far from the predictions. This means that, at the beginning of the training, the loss landscape is built in a way that the PINN directs its training towards solutions that are closely aligned with the data. For a higher regularization value ($\eta_r = 5000$), the PINN predicts the TG concentration with satisfaction to the physics, meaning that the rate constants predicted by the PINN fit adequately the governing equations encoded within its training.

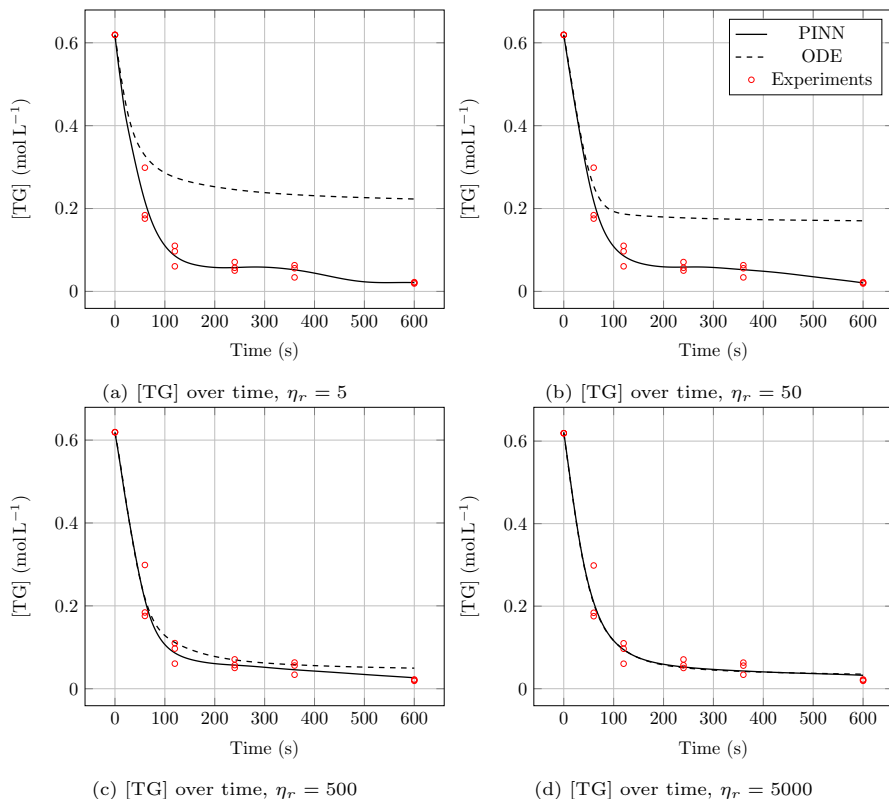


Figure 4: Impact of the regularization η_r on the predictions of the concentration of triglycerides and on the evaluation of the rate constants. Experiments used were carried out with a power of 4 W.

In Figure 5, we present the predictions of the temperature evolution over time made by the PINN and we compare them to the microwave data. Note that the temperature data has a resolution of 1 °C and is displayed each second of the reaction, creating discontinuous steps in the temperature monitoring. With the ODE describing the overall energy balance of the reactor, the PINN makes the temperature output smoother. Moreover, with a reduced η_g value, the evolution of the temperature does not follow a perfect quadratic equation, as suggested in Equation 21. Less severe regularization enables the predictions to deviate from the proposed ODE and align with the real data that capture physicochemical changes.

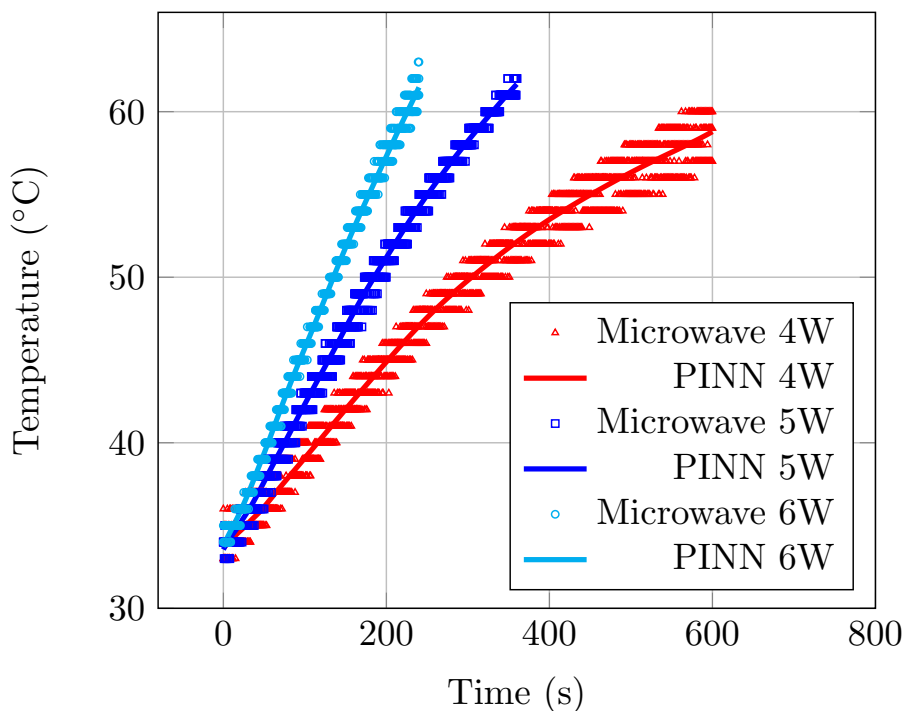


Figure 5: Temperature predicted by the PINN.

3.2. Identification of the system

In addition to predicting concentration and temperature, the PINN also assesses the unidentified parameters within the ODEs. The predicted rate constants k' and k'' for each reaction are presented in Table 4. With the use of Equation 19, it is possible to retrieve the pre-exponential factor A and the activation energy E_a . For the first forward reaction (conversion of triglycerides), A is approximately $1.1 \times 10^7 \text{ s}^{-1}$ and E_a is around 49 kJ mol^{-1} . Regarding the parameters within the energy balance, the PINN determines that the constants are set at 0.37 °C J^{-1} for ε , -0.01 s^{-1} for c_1 and -0.44 °C s^{-1} for c_2 .

Rate constant	Value (s ⁻¹)	Rate constant	Value (s ⁻¹ °C ⁻¹)
k_1'	0.104	k_1''	0.006
k_3'	0.116	k_3''	0.007
k_5'	0.095	k_5''	0.005
Rate constant	Value (L mol ⁻¹ s ⁻¹)	Rate constant	Value (L mol ⁻¹ s ⁻¹ °C ⁻¹)
k_2'	0.051	k_2''	0.003
k_4'	0.072	k_4''	0.004
k_6'	0.006	k_6''	0.000

Table 4: Rate constants predicted by the PINN.

Figure 6 shows the comparison between the normalized concentrations predicted by the PINN on one hand and the experiments on the other. We see that the majority of the PINN’s predictions are within the standard deviation error bars of the experiments. Less accurate predictions are made at the end and the beginning of the reaction, when the concentrations measured by the GC-FID carry a higher inherent uncertainty. Because we place more emphasis on penalization the ODEs using a severe regularization, it is expected that the PINN enforces the physics and produces solutions that satisfy the underlying ODEs.

Figure 7 shows the evolution of DG concentration over time using the PINN model at the end of its training (1M epochs). We compare the PINN’s predictions to the numerical solution of the ODEs for three different microwave power inputs (4, 5 and 6 W). We note that the PINN solves almost perfectly the ODEs while fitting the experimental data as closely as possible. Similar results are obtained with TG and MG. Indeed, the straight lines follow the dotted lines, meaning that the controlled regularization plays a major role in the training of the PINN. Without it, the PINN would not discover rate constants that are consistent with the predicted solution of the ODEs.

Finally, the architecture of the PINN influences the predictions. Firstly, adding the temperature as an output impacts the concentration predictions. Indeed, the fact that the loss function includes the temperature data and the residual of the energy balance changes the optimization problem of the PINN. Not only the PINN plays the role of a filter, but it also finds the best fit between the temperature and the concentration by leveraging the Arrhenius equation.

Secondly, using microwave power as an input makes a big difference in the results. This additional input results in a notable differentiation in the reaction kinetics observed during experiments conducted at 4, 5, and 6 W. The inclusion of the power input neuron empowers the network to elucidate the relationship between concentration and power, even though power is not directly linked to glycerides in the ODEs.

Overall, the most effective architecture involves setting the operating variables, like reaction time and microwave power, as the input neurons and the

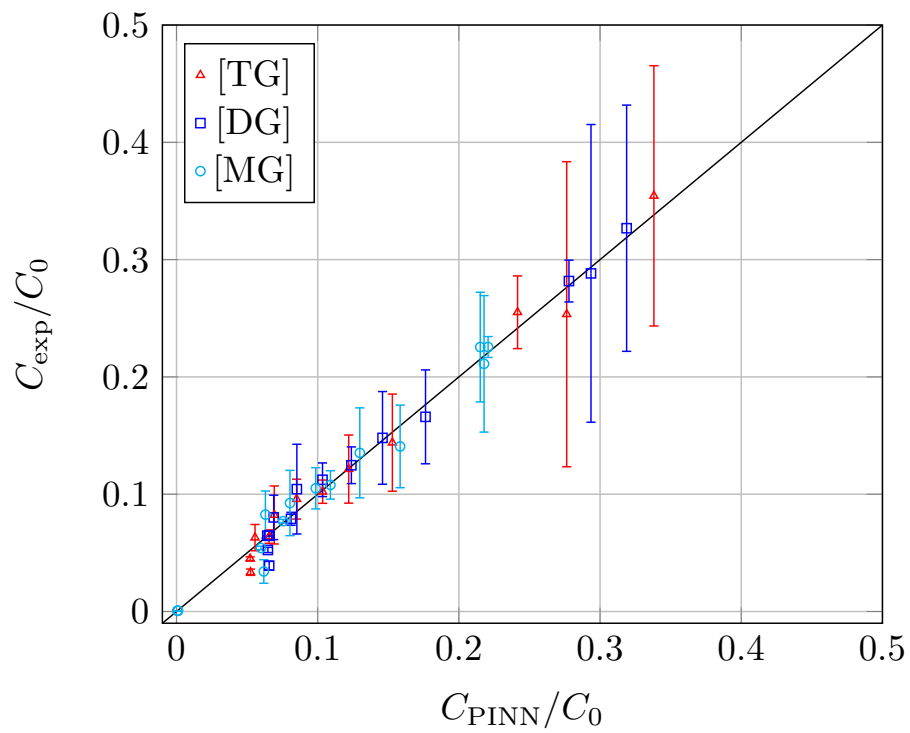


Figure 6: Parity plot between the concentration of glycerides C predicted by the PINN and the experimental results.

state variables, such as concentration and temperature, as the output variables. This arrangement of neurons results in more reliable predictions.

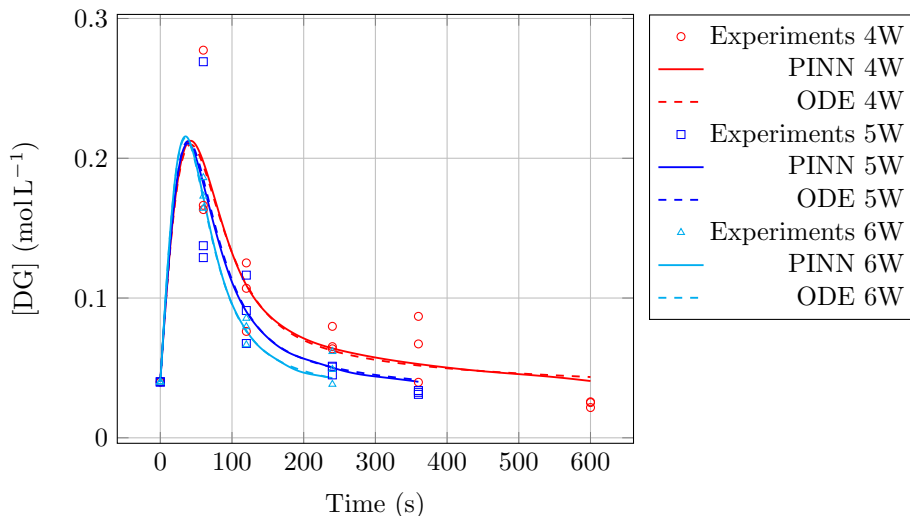


Figure 7: PINN’s predictions of the concentration of diglycerides over time compared to the numerical method and the experiments.

3.3. Extrapolation to conditions not trained for

We want to assess the capacity of the PINN to predict the rates of reactions that have unknown concentrations and have been performed under diverse operating conditions. To do so, we perform two different tests. For both tests, we train the 4, 5 and 6 W reactions by evaluating the loss of the ODEs describing the species balance (at the temporal collocation points), the loss of the ODE describing the energy balance (at the temporal collocation points) and the loss of the microwave temperature data (at each second of the reaction). For the first test, we add to the loss only the MSE of the 4 W concentration data, whereas for the second test, we add only the MSE of the 6 W concentration data.

Figure 8 shows the predictions of the DG concentration over time for the microwave power inputs of 5 and 6 W after training the PINN only with concentrations from the 4 W experiments. Figure 9 shows the same but for the microwave powers of 4 and 5 W after training only with concentrations from the 6 W experiments.

PINN’s predictions from Figure 8 are almost all within the error bars of the experiments, without ever seeing the concentration data. PINN’s predictions from Figure 9 are less consistent with the experiments. Similar results are obtained for TG and MG in both cases. The maximum reaction time of the 6 W experiments is 240 s, the time when the temperature reaches 65 °C and methanol starts to evaporate. Because no concentration data are available after this time, the PINN only fits the ODEs at the collocation points. The PINN finds easily

and rapidly a local minimum, where the concentration derivative is zero. That is why, from 240 s, all concentrations reach a plateau and do not predict accurately the experiments. Overall, if the PINN knows concentration data that cover all the time domain of the ODEs, the PINN successfully extrapolates, otherwise, it gets stuck in a local minimum.

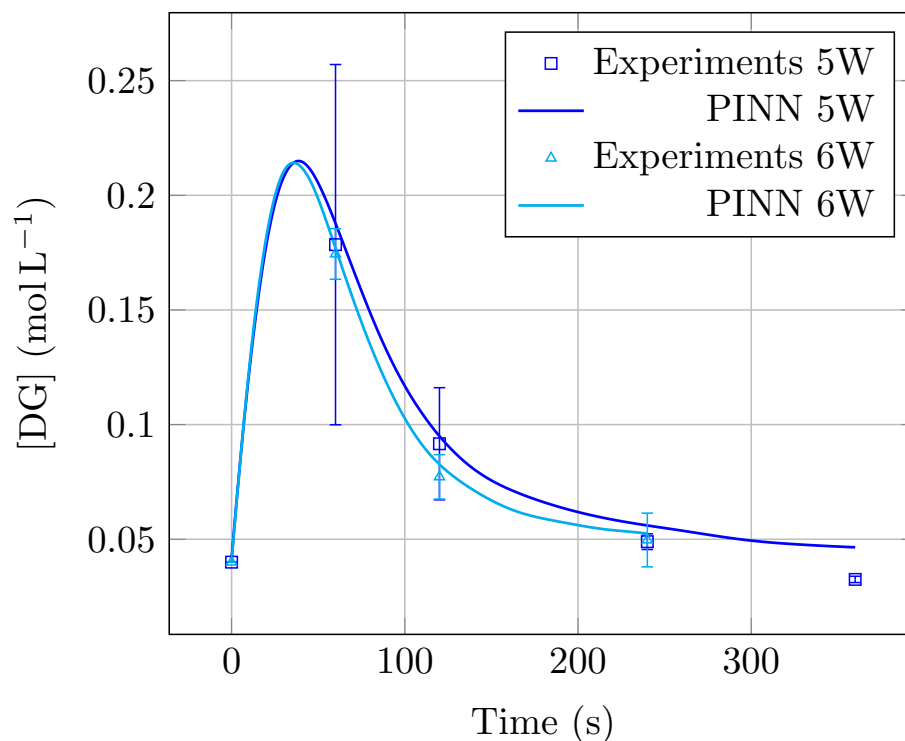


Figure 8: PINN’s predictions of the concentration of diglycerides over time with only data from 4 W are known during training.

4. Conclusion

In this work, we propose a PINN algorithm, which combines a mathematical model with experimental measurements, to predict the reaction rates of a biodiesel process using microwaves. The mathematical model consists of a system of ODEs, which incorporates rate laws, species balance and a linearized form of the Arrhenius equation. Experimental measurements involve obtaining the products’ temperature from the IR sensor of the microwave reactor and the glycerides concentration using GC-FID. We train the PINN using a user-controlled regularization parameter so its predictions are close to the data while respecting the underlying ODEs.

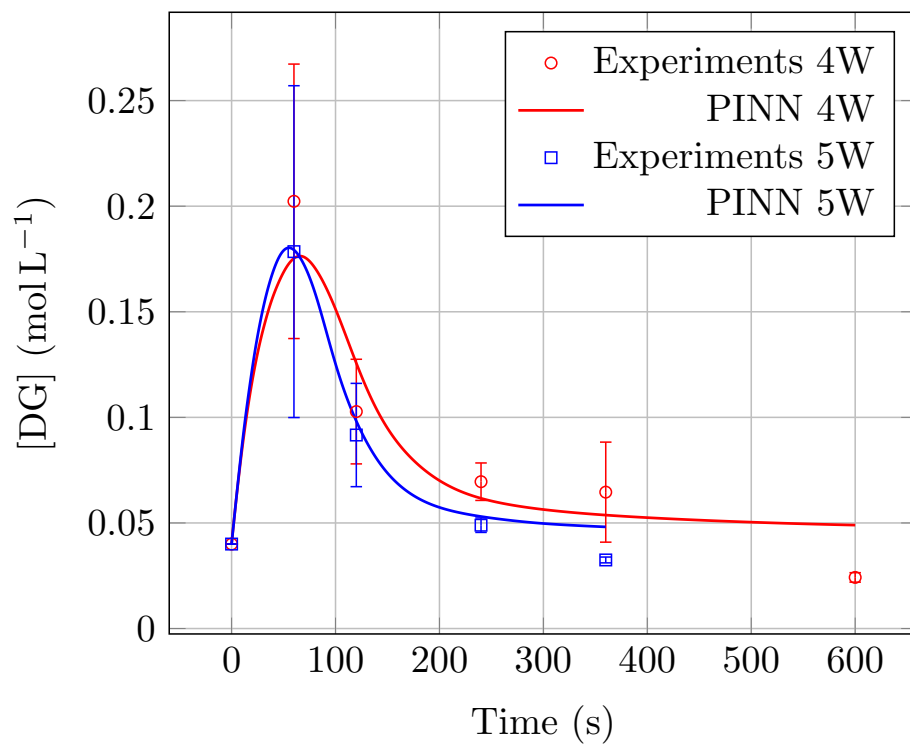


Figure 9: PINN's predictions of the concentration of diglycerides over time with only data from 6 W are known during training.

Results show that the PINN discovers rate constants k that satisfy the system of ODEs, predicts the species concentration as closely as possible to the experimental data and filters low-resolution temperature data. We also evaluate the ability of the PINN to extrapolate to operating conditions where concentration data are unknown. Results show that the PINN is able to predict concentrations within the error range of experiments that were not part of the training dataset. Based on these outcomes, we can conclude that with a set of ODEs, accessible temperature data and only a few concentration data of non-negligible errors, a PINN is able to identify the reaction kinetics of a biodiesel process and extend its predictions to other microwave powers.

The approach presented within this work can be used to identify unknown parameters of most ODEs. Therefore, PINNs can be easily adapted to any reactions by altering the ODEs within the loss function. However, once trained, a PINN is only valid for one specific set of reactions and one reacting system. If the reaction is changed, one would need to produce new experiments and train the PINN using these new data points.

Future work includes the addition of other features that have an impact on the reaction kinetics such as catalysis concentration, agitation speed and reaction volume. By adding more parameters to the design of experiments and to the inputs of the model, the PINN could formulate a full digital twin of the microwave reactor. Consequently, we strongly believe that this approach is viable to rapidly constitute a physics/data-driven hybrid model for intensified chemical reactors.

Acknowledgements

Valérie Bibeau would like to acknowledge financial support from the Natural Sciences and Engineering Research Council of Canada (NSERC) through the Canada Graduate Scholarships-Master’s Program. Bruno Blais would like to acknowledge the financial support from the Natural Sciences and Engineering Research Council of Canada (NSERC) through the RGPIN-2020-04510 Discovery Grant. This research was undertaken, in part, thanks to funding from the Canada Research Chair Program. The authors would also like to acknowledge technical support and computing time provided by the Digital Research Alliance of Canada and Calcul Québec. Computations were made on clusters Beluga managed by the Digital Research Alliance of Canada. The authors would like to acknowledge the efficient support received from Scion Instruments analysts for the GC-FID maintenance.

References

- [1] A. Stankiewicz, J. A. Moulijn, Process intensification, *Industrial & Engineering Chemistry Research* 41 (8) (2002) 1920–1924.
- [2] A. I. Stankiewicz, J. A. Moulijn, et al., Process intensification: transforming chemical engineering, *Chemical engineering progress* 96 (1) (2000) 22–34.

- [3] E. Pahija, S. Golshan, B. Blais, D. C. Boffito, Perspectives on the process intensification of co2 capture and utilization, *Chemical Engineering and Processing-Process Intensification* 176 (2022) 108958.
- [4] E. Thostenson, T.-W. Chou, Microwave processing: fundamentals and applications, *Composites Part A: Applied Science and Manufacturing* 30 (9) (1999) 1055–1071.
- [5] S. Nomanbhay, M. Y. Ong, A review of microwave-assisted reactions for biodiesel production, *Bioengineering* 4 (2) (2017) 57.
- [6] C. S. Lee, E. Binner, C. Winkworth-Smith, R. John, R. Gomes, J. Robinson, Enhancing natural product extraction and mass transfer using selective microwave heating, *Chemical Engineering Science* 149 (2016) 97–103.
- [7] H. C. Foley, *Introduction to Chemical Engineering Analysis Using Mathematics: For Chemists, Biotechnologists and Materials Scientists*, Academic Press, 2021.
- [8] I. C. Romero-Ibarra, A. M. P. Escuela, G. E. M. Zúñiga, W. E. M. Muñoz, Direct transesterification: From seeds to biodiesel in one-step using homogeneous and heterogeneous catalyst, in: D. I. Fattah (Ed.), *Advanced Biodiesel - Technological Advances, Challenges, and Sustainability Considerations*, IntechOpen, Rijeka, 2022, Ch. 5. doi:10.5772/intechopen.108234. URL <https://doi.org/10.5772/intechopen.108234>
- [9] A. Abbaszaadeh, B. Ghobadian, M. R. Omidkhah, G. Najafi, Current biodiesel production technologies: A comparative review, *Energy Conversion and Management* 63 (2012) 138–148.
- [10] N. Azcan, A. Danisman, Alkali catalyzed transesterification of cottonseed oil by microwave irradiation, *Fuel* 86 (17-18) (2007) 2639–2644.
- [11] K. Thakkar, S. S. Kachhwaha, P. Kodgire, A novel approach for improved in-situ biodiesel production process from gamma-irradiated castor seeds using synergistic ultrasound and microwave irradiation: Process optimization and kinetic study, *Industrial Crops and Products* 181 (2022) 114750.
- [12] D. Himmelblau, C. Jones, K. Bischoff, Determination of rate constants for complex kinetics models, *Industrial & Engineering Chemistry Fundamentals* 6 (4) (1967) 539–543.
- [13] L. P. de Oliveira, D. Hudebine, D. Guillaume, J. J. Verstraete, A review of kinetic modeling methodologies for complex processes, *Oil & Gas Science and Technology–Revue d’IFP Energies nouvelles* 71 (3) (2016) 45.
- [14] A. F. Aguilera, P. Tolvanen, K. Eränen, J. Wärnä, S. Leveneur, T. Marchant, T. Salmi, Kinetic modelling of prileschajew epoxidation of oleic acid under conventional heating and microwave irradiation, *Chemical Engineering Science* 199 (2019) 426–438.

- [15] K. Thakkar, A. Vhora, P. Kodgire, S. S. Kachhwaha, Effectiveness of rsm based box behnken doe over conventional method for process optimization of biodiesel production, in: *Mathematical Modeling, Computational Intelligence Techniques and Renewable Energy: Proceedings of the First International Conference, MMCITRE 2020*, Springer, 2021, pp. 161–173.
- [16] W. H. Green, Moving from postdictive to predictive kinetics in reaction engineering, *MIT Open Access Articles* (2020).
- [17] C. Sun, V. G. Shi, Physinet: A combination of physics-based model and neural network model for digital twins, *International Journal of Intelligent Systems* 37 (8) (2022) 5443–5456.
- [18] L. Wright, S. Davidson, How to tell the difference between a model and a digital twin, *Advanced Modeling and Simulation in Engineering Sciences* 7 (1) (2020) 1–13.
- [19] D. Jones, C. Snider, A. Nassehi, J. Yon, B. Hicks, Characterising the digital twin: A systematic literature review, *CIRP journal of manufacturing science and technology* 29 (2020) 36–52.
- [20] F. Tao, B. Xiao, Q. Qi, J. Cheng, P. Ji, Digital twin modeling, *Journal of Manufacturing Systems* 64 (2022) 372–389.
- [21] S. Cuomo, V. S. Di Cola, F. Giampaolo, G. Rozza, M. Raissi, F. Piccialli, Scientific machine learning through physics-informed neural networks: where we are and what’s next, *Journal of Scientific Computing* 92 (3) (2022) 88.
- [22] M. Raissi, P. Perdikaris, G. E. Karniadakis, Physics-informed neural networks: A deep learning framework for solving forward and inverse problems involving nonlinear partial differential equations, *Journal of Computational physics* 378 (2019) 686–707.
- [23] A. G. Baydin, B. A. Pearlmutter, A. A. Radul, J. M. Siskind, Automatic differentiation in machine learning: a survey, *Journal of Machine Learning Research* 18 (2018) 1–43.
- [24] I. Goodfellow, Y. Bengio, A. Courville, *Deep learning*, MIT press, 2016.
- [25] S. I. Ngo, Y.-I. Lim, Solution and parameter identification of a fixed-bed reactor model for catalytic co2 methanation using physics-informed neural networks, *Catalysts* 11 (11) (2021) 1304.
- [26] C. O. Kappe, My twenty years in microwave chemistry: from kitchen ovens to microwaves that aren’t microwaves, *The chemical record* 19 (1) (2019) 15–39.

- [27] A. J. Folayan, P. A. L. Anawe, A. E. Aladejare, A. O. Ayeni, Experimental investigation of the effect of fatty acids configuration, chain length, branching and degree of unsaturation on biodiesel fuel properties obtained from lauric oils, high-oleic and high-linoleic vegetable oil biomass, *Energy Reports* 5 (2019) 793–806.
- [28] F. Qiu, Y. Li, D. Yang, X. Li, P. Sun, Biodiesel production from mixed soybean oil and rapeseed oil, *Applied Energy* 88 (6) (2011) 2050–2055.
- [29] O. S. Stamenković, M. Lazić, Z. Todorović, V. Veljković, D. Skala, The effect of agitation intensity on alkali-catalyzed methanolysis of sunflower oil, *Bioresource technology* 98 (14) (2007) 2688–2699.
- [30] D. Frascari, M. Zuccaro, A. Paglianti, D. Pinelli, Optimization of mechanical agitation and evaluation of the mass-transfer resistance in the oil transesterification reaction for biodiesel production, *Industrial & Engineering Chemistry Research* 48 (16) (2009) 7540–7549.
- [31] D. Y. Leung, X. Wu, M. K. H. Leung, A review on biodiesel production using catalyzed transesterification, *Applied energy* 87 (4) (2010) 1083–1095.
- [32] G. Knothe, Analyzing biodiesel: standards and other methods, *Journal of the American Oil Chemists' Society* 83 (10) (2006) 823–833.
- [33] E. C. for Standardization (CEN), En 14105: Fat and oil derivatives. fatty acid methyl esters (fame). determination of free and total glycerol and mono-, di-, triglyceride contents (reference method) (2011).
- [34] H. Laajimi, F. Galli, G. S. Patience, D. Schieppati, Experimental methods in chemical engineering: Gas chromatography—gc, *The Canadian Journal of Chemical Engineering* 100 (11) (2022) 3123–3144.
- [35] D. Zeng, R. Li, T. Jin, T. Fang, Calculating the thermodynamic characteristics and chemical equilibrium of the stepwise transesterification of triolein using supercritical lower alcohols, *Industrial & Engineering Chemistry Research* 53 (17) (2014) 7209–7216.
- [36] F. Trejo-Zárraga, F. de Jesús Hernández-Loyo, J. C. Chavarría-Hernández, R. Sotelo-Boyás, Kinetics of transesterification processes for biodiesel production, *Biofuels-State of development* (2018) 149–179.
- [37] M.-C. Hsiao, P.-H. Liao, N. V. Lan, S.-S. Hou, Enhancement of biodiesel production from high-acid-value waste cooking oil via a microwave reactor using a homogeneous alkaline catalyst, *Energies* 14 (2) (2021) 437.
- [38] B. Likozar, J. Levec, Transesterification of canola, palm, peanut, soybean and sunflower oil with methanol, ethanol, isopropanol, butanol and tert-butanol to biodiesel: Modelling of chemical equilibrium, reaction kinetics and mass transfer based on fatty acid composition, *Applied energy* 123 (2014) 108–120.

- [39] S. Wang, Y. Teng, P. Perdikaris, Understanding and mitigating gradient flow pathologies in physics-informed neural networks, *SIAM Journal on Scientific Computing* 43 (5) (2021) A3055–A3081.
- [40] Y. Yang, P. Perdikaris, Adversarial uncertainty quantification in physics-informed neural networks, *Journal of Computational Physics* 394 (2019) 136–152.
- [41] A. Krishnapriyan, A. Gholami, S. Zhe, R. Kirby, M. W. Mahoney, Characterizing possible failure modes in physics-informed neural networks, *Advances in Neural Information Processing Systems* 34 (2021) 26548–26560.
- [42] D. P. Kingma, J. Ba, Adam: A method for stochastic optimization, arXiv preprint arXiv:1412.6980 (2014).
- [43] V. Bibeau, *lethe-cfd/bio-pinn* (2023).
URL <https://github.com/lethe-cfd/bio-pinn>
- [44] U. M. Ascher, L. R. Petzold, *Computer methods for ordinary differential equations and differential-algebraic equations*, Vol. 61, Siam, 1998.
- [45] K. Prantikos, L. H. Tsoukalas, A. Heifetz, Physics-informed neural network solution of point kinetics equations for a nuclear reactor digital twin, *Energies* 15 (20) (2022) 7697.
- [46] W. Ji, W. Qiu, Z. Shi, S. Pan, S. Deng, Stiff-pinn: Physics-informed neural network for stiff chemical kinetics, *The Journal of Physical Chemistry A* 125 (36) (2021) 8098–8106.